

AMP: Autoregressive Motion Prediction Revisited with Next Token Prediction for Autonomous Driving

Xiaosong Jia¹ Shaoshuai Shi^{3†} Zijun Chen¹ Li Jiang⁴
Wenlong Liao^{1,2} Tao He² Junchi Yan^{1†}

1. Department of CSE, Shanghai Jiao Tong University
 2. Cowa Robot
 3. Max Planck Institute for Informatics
 4. The Chinese University of Hong Kong, Shenzhen
- † Correspondence authors

Abstract. As an essential task in autonomous driving (AD), motion prediction aims to predict the future states of surround objects for navigation. One natural solution is to estimate the position of other agents in a step-by-step manner where each predicted time-step is conditioned on both observed time-steps and previously predicted time-steps, i.e., autoregressive prediction. Pioneering works like SocialLSTM and MFP design their decoders based on this intuition. However, almost all state-of-the-art works assume that all predicted time-steps are independent conditioned on observed time-steps, where they use a single linear layer to generate positions of all time-steps simultaneously. They dominate most motion prediction leaderboards due to the simplicity of training MLPs compared to autoregressive networks.

In this paper, we introduce the GPT style next token prediction into motion forecasting. In this way, the input and output could be represented in a unified space and thus the autoregressive prediction becomes more feasible. However, different from language data which is composed of homogeneous units -words, the elements in the driving scene could have complex spatial-temporal and semantic relations. To this end, we propose to adopt three factorized attention modules with different neighbors for information aggregation and different position encoding styles to capture their relations, *e.g.*, encoding the transformation between coordinate systems for spatial relativity while adopting RoPE for temporal relativity. Empirically, by equipping with the aforementioned tailored designs, the proposed method achieves state-of-the-art performance in the Waymo Open Motion and Waymo Interaction datasets. Notably, AMP outperforms other recent autoregressive motion prediction methods: MotionLM and StateTransformer, which demonstrates the effectiveness of the proposed designs.

Keywords: Motion Prediction · Autonomous Driving · Autoregressive Generation

1 Introduction

Motion forecasting is one key module of a modern autonomous driving (AD) system, which aims to predict the positions of surrounding agents in the next few time-steps so that its downstream module - planner could generate safe route for the ego vehicle without collisions. As the prediction interval could be long (for example, 8 seconds in Waymo Open Motion [6]), one natural idea is to generate the whole sequence in a step-by-step manner, *i.e.*, autoregressive prediction. Mathematically, autoregressive prediction is defined as: given the observed state \mathbf{S}_{obs} and t already predicted states $\{\mathbf{S}_1, \dots, \mathbf{S}_t\}$, the state at $t + 1$ is estimated conditioned both on \mathbf{S}_{obs} and $\{\mathbf{S}_1, \dots, \mathbf{S}_t\}$. Mathematically, for each sampled mode, the whole predicted sequence under *autoregressive setting* with length T is generated as in Eq. 1:

$$P(\mathbf{S}_1, \dots, \mathbf{S}_T | \mathbf{S}_{\text{obs}}) = \prod_{t=1}^T P(\mathbf{S}_t | \mathbf{S}_1, \dots, \mathbf{S}_{t-1}, \mathbf{S}_{\text{obs}}) \quad (1)$$

Since autoregressive prediction fits the intuition that people in the real world move in a *think-act-think-act* circle, pioneering works in the motion prediction field like Social LSTM [1] and MFP [44] adopt this setting. They combine the recurrent neural network (RNN) and conditional variational auto encoder (CVAE) as their decoder to generate the future trajectory step-by-step.

However, as pointed out by existing literatures [17], due to the recurrent nature and the variational inference process of their methods, they suffer from training instability and have difficulty to capture the long-term dependency. As a result, among state-of-the-art works [28, 36, 53] which dominate widely used large-scale autonomous driving motion prediction datasets [6, 50], they all adopt the simplified assumption that *all future time-steps are independent conditioned on the observed time-steps*. Mathematically, for each sampled mode, the whole predicted sequence under *independent setting* with length T is generated as in Eq. 2:

$$P(\mathbf{S}_1, \dots, \mathbf{S}_T | \mathbf{S}_{\text{obs}}) = \prod_{t=1}^T P(\mathbf{S}_t | \mathbf{S}_{\text{obs}}) \quad (2)$$

Compared to autoregressive generation, independent generation could overcome the long-term dependency and optimization issues caused by autoregressive RNN due to the fact that every predicted time-step only depends on \mathbf{S}_{obs} which is input without any cumulative errors. Considering its simplicity and convenience to implement and train, lots of methods are developed based on it including winner solutions [5, 10, 25, 36, 49, 54] of multiple competitions.

Nevertheless, in the NLP field, the Seq2Seq [4, 43] model has been eventually replaced by GPT [2, 34], partly due to the homogeneous representation of GPT for both inputs and outputs (words) which best describes the inherent characteristics of the language data. In this work, we aim to take a similar step: representing the movement of agents in a unified feature space. Notably, recent works [20, 38, 53] have suggested that normalizing the observed states of

agents, i.e., inputs, into the ego-centric representation would enhance the performance. Different from previous works, we transform both the observed states and future states into ego-centric tokens and adopt the GPT style next token prediction training. Further, different from pure language data, the autonomous driving scene is heterogeneous, i.e., elements have multiple types and complex spatial-temporal relations. To this end, we propose multiple tailored designs: (i) We use different tokenizers and attention networks for map and agents. (ii) We use RoPE [40], the state-of-the-art relative position embedding, to capture the temporal relativity among tokens of same agents. (iii) We encode the transformations between coordinate systems, similar to [20,38,53], as the relative spatial position encoding for the tokens at the same time-step. After the aforementioned adaptations, the proposed autoregressive motion prediction model, called **AMP**, achieves state-of-the-art performance on the Waymo Open Motion and Waymo Interaction datasets. In summary, our contributions are:

- We propose an autoregressive prediction paradigm for motion forecasting. Under this setting, the inputs and outputs are unified into the same representation space, which could fully utilize the information of whole sequence.
- Tailored for the complex spatial-temporal and semantic relations among elements in the driving scene, we design different attention mechanisms and relative position encodings to capture these priors.
- The proposed model achieves state-of-the-art performance on the Waymo Open Motion and Waymo Interaction datasets. **Notably, AMP outperforms other recent autoregressive motion prediction methods: MotionLM and StateTransformer.**

2 Related Works

2.1 GPT Style Modeling

Transformer [48], with its general design to process information and scalable architecture, has revolutionized the deep learning field. The recent huge success of ChatGPT [2,30] shows the power of next token prediction as a proxy task, which unifies the input and output space. Similar efforts have been made in multiple fields, such as vision [3], VQA [30], robotics [56], protein [7], all of which demonstrate strong performance.

2.2 Motion Prediction

One intuitive way to conduct motion prediction is to generate the future states in a step-by-step way so that each step is consistent with the previous generated steps. In pioneering learning-based works, they design their decoder based on this intuition. Social LSTM [1] directly fed the predicted step into LSTM [12] during training and Social GAN [11] further adds an adversarial recurrent discriminator to enhance diversity. DESIRE [21] and MFP [44] adopt the probabilistic latent variable generative model based on CVAE and their training maximizes a variational lower bound on the log-likelihood of data. However, due to the cumulative error issue and difficulty to optimize [17], later

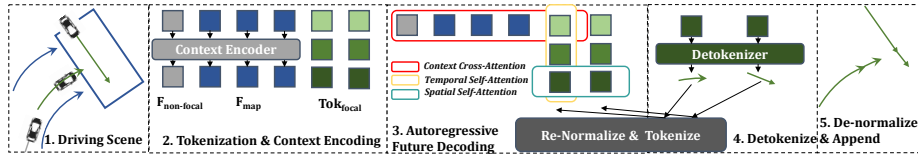


Fig. 1: Overall Paradigm of AMP. First, we normalize and tokenize all elements in the scene in Sec. 3.2 and use Context Encoder to encode the static map elements and non-focal agents in Sec. 3.3. Then, we conduct three different attention mechanisms in Future Decoder to autoregressively generate future trajectories in Sec. 3.4. Next, we detokenize the predicted token into future trajectories in Sec. 3.5. Finally, we re-normalize and tokenize the predicted trajectories for future generation in Sec. 3.7.

works [9, 15, 18, 19, 22, 24, 27, 51] make the assumption that for each mode, all future time-steps are independent conditioned on observed time-steps and thus they could use an MLP to generate all future states simultaneously. Though counter-intuitive, methods based on this design could outperform the autoregressive prediction model a lot. As a result, state-of-the-art works [36, 38, 53] and competition winners [5, 10, 25, 49, 54] all follow this design. Notably, Scene-Transformer [29] treats each input time-step as a token and conducts factorized spatial-temporal attention among observed states of agents. However, they still use an MLP to generate future trajectories. Additionally, since they use a scene-centric representation and thus the representation space of tokens are not unified. Later, there are works to discuss the importance of unified representation, i.e. ego-centric normalization [20, 38, 55]. Nevertheless, their unification are still only for inputs ignoring the homology between input and output.

3 Method

3.1 Problem Formulation

The input of the motion prediction task includes (1) the observed states of surrounding agents (vehicles, pedestrians, cyclist, etc) as $\mathbf{S}_{\text{obs}} \in \mathbb{R}^{N_{\text{agent}} \times T_{\text{obs}} \times H_{\text{agent}}}$ where N_{agent} is the total number of agents, T_{obs} is the number of observed time-steps, and H_{agent} is the dimension of recorded state at each time-step (position, velocity, heading, etc) and (2) surrounding map elements $\mathbf{S}_{\text{map}} \in \mathbb{R}^{N_{\text{map}} \times L_{\text{map}} \times H_{\text{map}}}$ where N_{map} is the number of map elements, L_{map} is the number of points per polyline, and H_{map} is the hidden dimension of each point.

The motion prediction task aims to predict the future states of safety-critical focal agents $\mathbf{S}_{\text{future}} \in \mathbb{R}^{N_{\text{focal}} \times T_{\text{future}} \times H_{\text{target}}}$ where N_{focal} is the number of selected focal agents, T_{future} is the number of future time-steps to predict, and H_{target} is the dimension of the prediction at each future time-step.

Different from previous works where they only use the observed states as the inputs of the neural network for training, in this work, we adopt the GPT style next token prediction training strategy. Specifically, during training, both observed and future states of agents are tokenized, then fed into the neural network to perform next token prediction, and finally de-tokenized into predicted states. Fig. 1 demonstrates the overall paradigm of the proposed AMP.

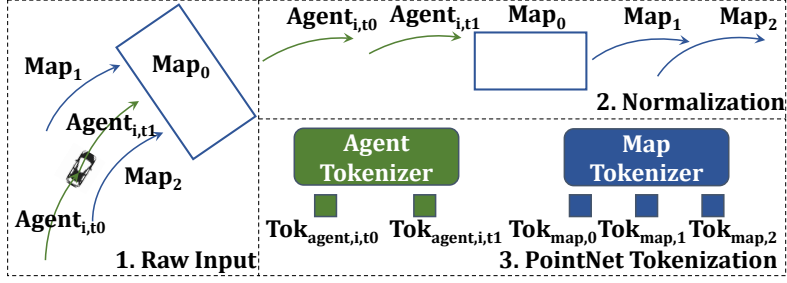


Fig. 2: Illustration of the Discretization & Tokenization Process. All elements are first normalized into ego-centric coordinate system within each small interval and then processed by type-specific PointNet to generate their corresponding tokens.

3.2 Discretization & Tokenization

In this step, we transform all heterogeneous inputs into a normalized and unified representation space. We demonstrate the procedure in Fig. 2.

Map Tokens: For all map elements, since they are all abstracted as polylines or polygons, we transform their reference coordinate system with origin at the first point and the positive x-axis aligning with the direction from the first to second point. Then, we use a VectorNet [8] style PointNet [33] to encode the normalized polylines/polygons. We denote the map tokens as $\mathbf{Tok}_{\text{map}} \in \mathbb{R}^{N_{\text{map}} \times H}$ where H is the hidden dimension of the model.

Agent Tokens: Different from map elements which are all static, agents usually have a long temporal interval (*e.g.*, in 10 Hz frequency, 1.1 second observed states and 8 second future states in Waymo Open Motion Dataset). Thus, we need to divide each agent into several equally-spaced tokens in the temporal dimension. Considering we only have the observed states as inputs during inference, the temporal length T_{token} of each token should be shorter than T_{obs} so that there is at least one token to be the input during inference. As a result, for each agent, we would have $L_{\text{obs}} = T_{\text{obs}}/T_{\text{token}}$ observed tokens and $L_{\text{future}} = T_{\text{future}}/T_{\text{token}}$ future tokens. Next, for each divided small temporal intervals of each agent, we normalize it by setting the reference coordinate system’s origin and positive x-axis as the position and heading of agent at the final time-step of the interval. Finally, we use another PointNet shared by all agents and intervals to encode them into observed agent tokens $\mathbf{Tok}_{\text{obs}} \in \mathbb{R}^{N_{\text{agent}} \times L_{\text{obs}} \times H}$ and future agent tokens $\mathbf{Tok}_{\text{future}} \in \mathbb{R}^{N_{\text{focal}} \times L_{\text{future}} \times H}$. Note that for non-focal agents, *i.e.*, those agents regarded as not interesting or not safety-critical by the datasets [6, 50], we do not calculate their future tokens to save the computation. Since we would only predict focal agents’ future, we re-organize these tokens by agents $\mathbf{Tok}_{\text{non-focal}} \in \mathbb{R}^{N_{\text{non-focal}} \times L_{\text{obs}} \times H}$ and $\mathbf{Tok}_{\text{focal}} \in \mathbb{R}^{N_{\text{focal}} \times (L_{\text{obs}} + L_{\text{future}}) \times H}$.

In summary, after this step, we would have the tokenized and normalized representations of the scene $\mathbf{Tok}_{\text{map}}$, $\mathbf{Tok}_{\text{focal}}$, and $\mathbf{Tok}_{\text{non-focal}}$.

Different from the homogeneous language data, these tokens have complex spatial-temporal and semantic relations which could not be handled by single

self-attention layers. Thus, we adopt a factorized design where tokens attend to different neighbors in different modules instead of being simply put together.

3.3 Context Encoder

Since $\mathbf{Tok}_{\text{map}}$ and $\mathbf{Tok}_{\text{non-focal}}$ are all fully observable during both training and inference, they could be seen as a **fixed context**. To reduce the computational burden, **we pre-compute them with the Context Encoder and then cache them** so that all $\mathbf{Tok}_{\text{focal}}$ could directly conduct cross-attention to them later. Otherwise, the length of sequence for each focal agent would be much longer (for example, in Waymo Open Motion, there could be thousands of context tokens).

As for the implementation of the Context Encoder, following MTR [36], we conduct top-k self-attention among $\mathbf{Tok}_{\text{map}}$ and $\mathbf{Tok}_{\text{non-focal}}$. Since all tokens’ features are in their own ego-centric coordinate system originally, we need to encode their spatial relations. To this end, we concatenate the relative spatial position encodings [20, 38, 53] with the token feature maps during attention process. Specifically, assume the references of the coordinate system for elements i, j are (x_i, y_i, θ_i) and (x_j, y_j, θ_j) respectively, then the relative spatial relations from i to j is $\Delta_{i \rightarrow j} = (x_j - x_i, y_j - y_i, \theta_j - \theta_i)$. Following NeRF [26], we adopts Fourier encoding and then an MLP to encode it as in Eq. 3:

$$\mathbf{Pos}_{i;j} = \text{MLP}_{\text{pos}}(\text{Fourier}(\Delta_{i \rightarrow j})) \quad (3)$$

where $\mathbf{Pos}_{i;j}$ is the relative spatial position embedding from element i to j .

In summary, the attention in Context Encoder works as in Equ. 4:

$$\begin{aligned} \mathbf{F}_i &= \text{MHA}(Q = [\mathbf{Tok}_i; \mathbf{Pos}_{i;\text{Neighbor}(i)}], \\ K &= [\mathbf{Tok}_{\text{Neighbor}(i)}; \mathbf{Pos}_{\text{Neighbor}(i);i}], \\ V &= [\mathbf{Tok}_{\text{Neighbor}(i)}; \mathbf{Pos}_{\text{Neighbor}(i);i}]) \end{aligned} \quad (4)$$

where \mathbf{F}_i is the updated feature for token i in $\mathbf{Tok}_{\text{map}}$ or $\mathbf{Tok}_{\text{non-focal}}$, MHA denotes the multi-head attention operation in Transformer [48], $[\cdot; \cdot]$ represents the feature concatenation, $\text{Neighbor}(i)$ denotes the top-k spatially nearest neighbors of token i , and $\mathbf{Pos}_{i;\text{Neighbor}(i)}$ denotes the relative spatial position embedding matrix between element i and all its neighbors. Note that we also use other structures of Transformer including LayerNorm, residual connection, and feed-forward network. After stacking multiple layers of Context Encoder, we cache the updated feature of $\mathbf{Tok}_{\text{map}}$ and $\mathbf{Tok}_{\text{non-focal}}$ as \mathbf{F}_{map} and $\mathbf{F}_{\text{non-focal}}$.

At the end of the Context Encoder, to provide more supervisions for $\mathbf{F}_{\text{non-focal}}$, we also adopts the dense future prediction module in [36], where we predict a rough future trajectories for all non-focal agents and then concatenate them with $\mathbf{F}_{\text{non-focal}}$ followed by an MLP.

3.4 Future Decoder

Future Decoder aims to aggregate the spatial-temporal information among $\mathbf{Tok}_{\text{focal}}$ and from context tokens \mathbf{F}_{map} and $\mathbf{F}_{\text{non-focal}}$. At each layer of the Fu-

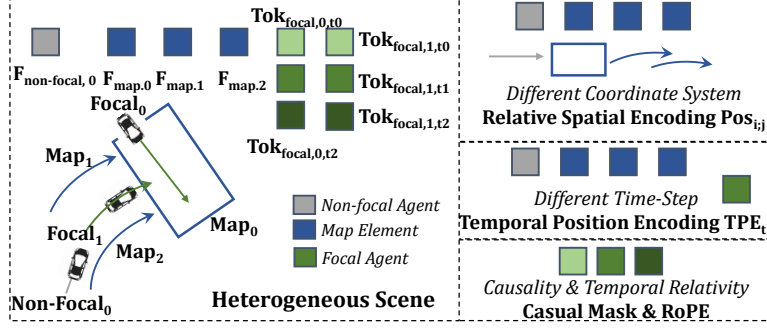


Fig. 3: Diverse Relations among Driving Scene and Corresponding Position Encodings. In all attention modules, the coordinate system is different among agents, which requires the Relative Spatial Position Encoding in Eq. 3. For the Context Cross Attention, to let the tokens of focal agents be aware of the temporal difference from the start time-step, we use the Temporal Position Encoding. For the Temporal Self-Attention, to capture the temporal relativity and avoid information leakage, we adopt the state-of-the-art designs for GPT - Causal Mask & RoPE.

ture Decoder, we employ three attention mechanisms for $\mathbf{Tok}_{\text{focal}}$ with different parameters, neighbors as introduced in following paragraphs.

Context Cross-Attention. For each focal agent at each time-step, **their future movement are influenced by the surrounding environments.** In Context Cross-Attention module, we let $\mathbf{Tok}_{\text{focal}}$ attend to the aforementioned cached and shared context tokens \mathbf{F}_{map} and $\mathbf{F}_{\text{non-focal}}$. Note that beside the difference of reference coordinate system mentioned in Sec. 3.3, there are temporal relativity as well. Specifically, all context tokens are captured at time-step T_{obs} while $\mathbf{Tok}_{\text{focal}}$ could be captured at the moment from T_{obs} to $T_{\text{obs}} + T_{\text{future}}$. To consider this factor, we additionally set a learnable temporal position embedding \mathbf{TPE} according to the discretized index of time-steps and add it to the query vector of $\mathbf{Tok}_{\text{focal}}$. Thus, the overall attention mechanism of Context Cross-Attention works as in Eq. 5:

$$\begin{aligned}
 \mathbf{F}_{\text{non-focal},i,t} &= \text{MHA}(Q = [\mathbf{Tok}_{i,t}; \mathbf{Pos}_{i,t;\text{non-focal}}] + \mathbf{TPE}_t, \\
 &\quad K = [\mathbf{F}_{\text{non-focal}}; \mathbf{Pos}_{\text{non-focal};i,t}], \\
 &\quad V = [\mathbf{F}_{\text{non-focal}}; \mathbf{Pos}_{\text{non-focal};i,t}]) \\
 \mathbf{F}_{\text{map},i,t} &= \text{MHA}(Q = [\mathbf{Tok}_{i,t}; \mathbf{Pos}_{i,t;\text{map}}] + \mathbf{TPE}_t, \\
 &\quad K = [\mathbf{F}_{\text{map}}; \mathbf{Pos}_{\text{map};i,t}], \\
 &\quad V = [\mathbf{F}_{\text{map}}; \mathbf{Pos}_{\text{map};i,t}])
 \end{aligned} \tag{5}$$

where $\mathbf{F}_{\text{non-focal},i,t}$ and $\mathbf{F}_{\text{map},i,t}$ are the retrieved features of focal agent i at time-step t about non-focal agents and maps respectively and $\mathbf{Pos}_{i,t;\text{non-focal}}$ and $\mathbf{Pos}_{\text{map};i,t}$ denote the relative spatial position encoding between focal agent i at time-step t and non-focal agents/maps respectively.

Temporal Self-Attention. During training, each focal agent has $L_{\text{obs}} + L_{\text{future}} = (T_{\text{obs}} + T_{\text{future}})/T_{\text{token}}$ temporal tokens. To enable the GPT style train-

ing of **next token prediction and avoid information leakage**, we apply the causal mask [2, 34] in the temporal self-attention module. Specifically, during training, each agent’s token at time-step t could only attend to the the agent’s token before time-step t . As for the position encoding, beside the spatial ones used in Eq. 3, there are temporal relativity among tokens as well. We require this position encoding could be the same for the same temporal gap. For example, the relative temporal encoding between time-step t and $t + 1$ should be the same with the one between time-step $t + 1$ and $t + 2$. To achieve this goal, we adopt the state-of-the-art relative encoding RoPE [40]. Concretely, RoPE is a kind of relative position embedding initially proposed in the NLP field, which combines the sinusoidal encoding with complex number and could be applied on Q and K separately. It is used in both GPT [2] and LLaMA [45, 46] and please refer to their paper for details [40]. In summary, the attention mechanism of Temporal Self-Attention is as in Eq. 6:

$$\begin{aligned}
 \mathbf{F}_{\text{temp},i,t} &= \text{MHA}(Q = \text{RoPE}([\mathbf{Tok}_{i,t}; \mathbf{Pos}_{i,t;i,\{0,\dots,t\}}]), \\
 &K = \text{RoPE}([\mathbf{Tok}_{i,\{0,\dots,t\}}; \mathbf{Pos}_{i,\{0,\dots,t\};i,t}], \\
 &V = [\mathbf{Tok}_{i,\{0,\dots,t\}}; \mathbf{Pos}_{i,\{0,\dots,t\};i,t}], \\
 &\text{AttentionMask} = \text{Causal})
 \end{aligned} \tag{6}$$

where $\mathbf{Tok}_{i,t}$ and $\mathbf{F}_{\text{temp},i,t}$ are the input and output features of focal agent i in time-step t for the causally temporal aggregation and $\mathbf{Pos}_{i,t;i,\{0,\dots,t\}}$ is the relative spatial position encoding matrix between focal agent i ’s at time-step t and all time-steps before it.

Spatial Self-Attention. During the selection of focal agents, the dataset builders [6, 50] usually combine some rules with manual checking to make sure these agents are interactive or safety-critical. To further **capture the potential complex interactions among focal agents**, Spatial Self-Attention module considers the spatial relation for focal agents at the same time-step. However, there is a train-val gap issue due to the multi-modality nature of motion prediction models. Specifically, during training, all focal agents are trained by the ground-truth mode, which is unique. During inference, since their future trajectories are generated in a step-by-step manner, each step has multiple possible modes which is different from training and thus it is unknown which mode of agent A should interact with which mode of agent B. To this end, we only conduct Spatial Self-Attention for observable time-steps which have an unique mode during both training and inference. In summary, the Spatial Self-Attention works as in Eq. 7:

$$\begin{aligned}
 \mathbf{F}_{\text{spatial},i,t} &= \text{MHA}(Q = [\mathbf{Tok}_{i,t}; \mathbf{Pos}_{i,t;\{0,\dots,N_{\text{focal}}\},t}], \\
 &K = [\mathbf{Tok}_{i,\{0,\dots,t\}}; \mathbf{Pos}_{\{0,\dots,N_{\text{focal}}\},t;i,t}], \\
 &V = [\mathbf{Tok}_{i,\{0,\dots,t\}}; \mathbf{Pos}_{\{0,\dots,N_{\text{focal}}\},t;i,t}]) \\
 &\text{where } t \leq t_{\text{obs}}
 \end{aligned} \tag{7}$$

where $\mathbf{Tok}_{i,t}$ and $\mathbf{F}_{\text{spatial},i,t}$ are the input and output of the Spatial Self-Attention for focal agent i at time-step t . $\mathbf{Pos}_{i,t;\{0,\dots,N_{\text{focal}}\},t}$ is the relative spatial position encoding between focal agent i at time-step t and all focal agents at time-step t .

Layer-Updating MLP. In the above paragraphs, we introduce three kinds of attention mechanisms in the Future Decoder. In each layer, these attention modules are conducted in parallel. Then, we concatenate all aggregated information - $\mathbf{F}_{\text{non-focal},i,t}$, $\mathbf{F}_{\text{map},i,t}$, $\mathbf{F}_{\text{temp},i,t}$, $\mathbf{F}_{\text{spatial},i,t}$ with the origin feature map $\mathbf{Tok}_{i,t}$ and feed them into an MLP to obtain the input for the next layer as in Eq. 8:

$$\mathbf{Tok}_{i,t}^{(l+1)} = \text{MLP}([\mathbf{Tok}_{i,t}^l; \mathbf{F}_{\text{non-focal},i,t}^l; \mathbf{F}_{\text{map},i,t}^l; \mathbf{F}_{\text{temporal},i,t}^l; \mathbf{F}_{\text{spatial},i,t}^l]) \quad (8)$$

where l is index of layer in the Future Decoder. In Fig. 3, we illustrate diverse relations in elements and the corresponding position encodings used for the attention among them.

3.5 Multi-Modal Detokenizer

After Future Decoder, focal agent tokens $\mathbf{Tok}_{\text{focal}}$ has aggregated spatial-temporal information from environment along with its ego movement. The Multi-Modal Detokenizer generates multiple possible futures based on $\mathbf{Tok}_{\text{focal}}$.

Inspired by the intuition that human moves with instant reactions under an ultimate goal, the Multi-Modal Detokenizer composes of **both short-term and long-term intention prediction and trajecotry generation**. Specifically, given $\mathbf{Tok}_{\text{focal}, i, t}$, we first distinguish its potential multi-modal long-term goals by concatenating with different embeddings as in Eq. 9:

$$\mathbf{Tok}_{\text{focal}, i, t}^k = [\mathbf{Tok}_{\text{focal}, i, t}; \mathbf{F}_{\text{long}}^k] \quad k \in \{1, \dots, K_{\text{long}}\} \quad (9)$$

where K_{long} is a hyper-parameter for the number of potential long-term goals and $\mathbf{F}_{\text{long}}^k$ is the learnable embedding for the goal k . In this work, we adopt the state-of-the-art anchor-based design [36] where the long-term goals are generated by k-means clustering of the normalized positions at T_{future} over the whole training set. Then, based on its long-term goals, agents should react to current environment. Here, we define the set of potential short-term goals as k-means clustering of the normalized positions at T_{token} . The short-term goal’s label is the one have shortest distance with the ground-truth. Thus, we could jointly train a short-term classifier $\text{CLS}_{\text{short}}$ and update the $\mathbf{Tok}_{\text{focal}, i, t}^k$ based on its short-term goals’ embeddings $\mathbf{F}_{\text{short}}$ as in Eq. 10:

$$\mathbf{Tok}_{\text{focal}, i, t}^{k'} = \text{MLP}_{\text{short}}([\text{CLS}_{\text{short}}(\mathbf{Tok}_{\text{focal}, i, t}^k) \cdot \mathbf{F}_{\text{short}}; \mathbf{Tok}_{\text{focal}, i, t}^k]) \quad (10)$$

where $\mathbf{Tok}_{\text{focal}, i, t}^{k'}$ is the feature containing information about long-term and short-term goals.

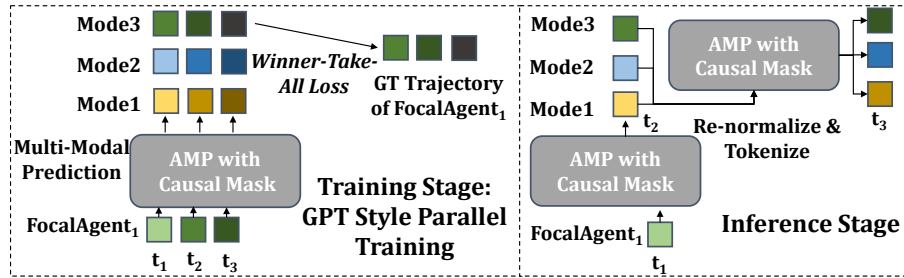


Fig. 4: Illustration of Training and Inference Stage of AMP. During training, we implement the GPT-style parallel training for all tokens of the temporal sequence of each focal agent. During inference, the input of the first time-step (observed) is unique while the rest are all autoregressively generated with multiple modes in parallel.

Finally, we use MLPs to decode the $\mathbf{Tok}_{\text{focal}, i, t}^{k'}$ into a concrete trajectory. Here, we still adopt the long-term plus short-term design. We use one MLP $\text{Dec}_{\text{short}}$ to generate the states in the next T_{token} steps $\hat{O}_{i,t,\text{short}}^k$ and another MLP Dec_{long} to generate the states in the next T_{future} steps $\hat{O}_{i,t,\text{long}}^k$. For inference, we combine the short-term predictions in the current time-step with the long-term predictions in the previous time-steps to generate the predictions $O_{i,t}^{k'}$ and then re-normalize it into its ego-centric coordinate system so that it could be fed back into the decoder autoregressively. The mechanism of the generation process is:

$$\begin{aligned}
 \hat{O}_{i,t,\text{short}}^k &= \text{Dec}_{\text{short}}(\mathbf{Tok}_{\text{focal}, i, t}^{k'}) \in \mathbb{R}^{T_{\text{token}} \times H_{\text{target}}} \\
 \hat{O}_{i,t,\text{long}}^k &= \text{Dec}_{\text{long}}(\mathbf{Tok}_{\text{focal}, i, t}^{k'}) \in \mathbb{R}^{T_{\text{future}} \times H_{\text{target}}} \\
 \hat{O}_{i,t}^k &= \text{Fuse}(\hat{O}_{i,t,\text{short}}^k, \{\hat{O}_{i,t',\text{long}}^k[t-t'] | t' \leq t\})
 \end{aligned} \tag{11}$$

where Fuse is the fusing function to integrate the current short-term prediction and history long-term prediction, which is weighted averaging in experiments.

Notably, one important advantage of the autoregressive prediction over the independent generation is that it estimates next states based on both existing predictions and the observation $P(\mathcal{S}_t | \mathcal{S}_1, \dots, \mathcal{S}_{t-1}, \mathcal{S}_{\text{obs}})$ instead of solely based on the observation $P(\mathcal{S}_t | \mathcal{S}_{\text{obs}})$. In the experiments, we find that the fusing of short-term and long-term prediction bring performance gains.

3.6 Objective Function

Following existing literatures [36], we adopt the winner-take-all type of loss and decouple the training objectives into regression and classification. Specifically, for both short-term $\hat{O}_{i,t,\text{short}}^{k'}$ and long-term prediction $\hat{O}_{i,t,\text{long}}^k$, we only back-propagate the regression loss for one mode, which is selected as the one having shortest distance with the pre-set anchors generated as in Sec. 3.5. The ground-truth of the classification task is set as the index of the selected mode. The overall loss function is as in Eq. 12:

$$\mathcal{L} = \text{Reg}_{\text{short}} + \text{Cls}_{\text{short}} + \text{Reg}_{\text{long}} + \text{Cls}_{\text{long}} + \text{Reg}_{\text{dense}} \tag{12}$$

where $\text{Reg}_{\text{dense}}$ is the dense regression loss mentioned in Sec. 3.3 and we omit the weight of each term for clarity. Note that all regression loss is calculated based on the normalized labels which are transformed into the ego-centric coordinate system for each agent i at each time-step t .

3.7 Autoregressive Inference

During inference time, the initial inputs are only \mathbf{S}_{map} and \mathbf{S}_{obs} without the future states $\mathbf{S}_{\text{future}}$. We first use Context Encoder to cache the shared context features \mathbf{F}_{map} and $\mathbf{F}_{\text{non-focal}}$. Then, we use Future Decoder and Multi-Modal Detokenizer to generate K_{long} possible trajectories for next T_{token} steps. Note that we cache all middle layer features of Future Decoder $\mathbf{Tok}_{\text{focal},i,t}^{(l)}$ which could be reused similar to KV-cache [32] in GPT. Since the second step, there are K_{long} temporal sequence decoded for each agent where tokens could only temporally attend to the tokens within the same mode. As for the generated trajectory in each step $\hat{\mathbf{O}}_{i,t}^k$, we need to re-normalize it since the prediction is conducted in the coordinate system at current time-step. Finally, we could feed it into the tokenizer to obtain $\mathbf{Tok}_{\text{focal},i,t+1}$ to start the generation of next step. The generation halts when reaching the temporal length required by the benchmark. Fig. 4 demonstrates the procedure of training and inference stage for comparison.

4 Experiments

4.1 Dataset

Waymo Open Motion Dataset: We use the largest open-sourced motion prediction dataset Waymo Open Motion Dataset (WOMD) [6]. For each sample, it gives 11 time-step as observation and the target is to predict the future 80 time-steps. Within each scene, there are up to 8 focal agents and up to 6 possible futures of each focal agent are allowed for evaluation.

Waymo Interaction Dataset: Similar to [35,38], we also conduct experiments on the Waymo Interaction Dataset, where all pairs of selected agents are highly interactive and the evaluation is conducted with joint metrics.

4.2 Metrics

We use the official metrics suggested by the WOMD and its online leaderboard: minADE, minFDE, MR, and mAP where mAP is the primary metric. MR and mAP measure the ability of covering the focal agent’s intentions where minADE and minFDE measure the step-wise errors. All metrics are measured under 2Hz, which means we need to only submit 16 points for the 8 seconds prediction. Please refer to [6] for more details.

4.3 Results

In Table 1 and Table 2, we compare the proposed **AMP** with state-of-the-art works. We could observe that:

- **AMP outperforms other recent autoregressive methods.** Both State-Transformer and MotionLM normalize tokens in the agent-level. In AMP, all

Table 1: Performance on Waymo Open Motion Dataset. \uparrow denotes the higher the better while \downarrow denotes the lower the better. Results with ensemble are in *gray*.

Split	Decoding	Methods	mAP \uparrow	minADE \downarrow	minFDE \downarrow	MR \downarrow
Test	Indep	SceneTransformer [29]	0.2788	0.6117	1.2116	0.1564
		HDGT [20]	0.2826	0.5703	1.1434	0.1444
		HPTR [52]	0.3904	0.5565	1.1393	0.1434
		<i>MultiPath++</i> [47]	<i>0.4092</i>	<i>0.5557</i>	<i>1.1577</i>	<i>0.1340</i>
		WayFormer Factorized [28]	0.4118	0.5447	1.1255	0.1229
		WayFormer Multi-Axis [28]	0.4190	0.5454	1.1280	0.1228
		MTR [36]	0.4129	0.6050	1.2207	0.1351
		MTR++ [38]	0.4329	0.5906	1.1939	0.1298
		MTRA [37]	0.4492	0.5640	1.1344	0.1160
	<i>MTR++_Ens</i> [38]	<i>0.4634</i>	<i>0.5581</i>	<i>1.1166</i>	<i>0.1122</i>	
Autoreg	MotionLM [35]	0.4364	0.5509	1.1199	0.1058	
	AMP (ours)	0.4334	0.6012	1.1918	0.1311	
Val	Autoreg	StateTransformer [42]	0.3300	0.7200	1.4400	0.1900
		AMP (ours)	0.4321	0.6124	1.2017	0.1352

Table 2: Performance on Waymo Interaction Dataset. \uparrow denotes the higher the better while \downarrow denotes the lower the better. Results with ensemble are in *gray*. For MotionLM in the val set, we choose their best ensemble results and single mdoel with 64 rollouts for fair comparison respectively.

Split	Decoding	Methods	mAP \uparrow	minADE \downarrow	minFDE \downarrow	MR \downarrow
Test	Indep	SceneTransformer [29]	0.1192	0.9774	2.1892	0.4942
		M2I [41]	0.1239	1.3506	2.8325	0.5538
		DenseTNT [10]	0.1647	1.417	2.4904	0.5350
		<i>JFP</i> [23]	<i>0.2050</i>	<i>0.8817</i>	<i>1.9905</i>	<i>0.4233</i>
		MTR [36]	0.2037	0.9181	2.0633	0.4411
		MTR++ [38]	0.2326	0.8795	1.9505	0.4143
		GameFormer [14]	0.1923	0.9721	2.2146	0.4933
	Autoreg	MotionLM [35]	0.2178	0.8911	2.0067	0.4115
AMP (ours)		0.2294	0.9073	2.0415	0.4212	
Val	Autoreg	MotionLM [42]	0.2150	0.8831	1.9825	0.4092
		MotionLM [42]	0.1585	1.0585	2.4411	0.5114
		AMP (ours)	0.2344	0.8910	2.0133	0.4172

tokens are in their ego-centric coordinate system and their relativity are encoded by transformations between coordinate systems. Moreover, MotionLM and StateTransformer both adopt the joint self-attention strategy which flattens all time-steps of all agents into one sequence and thus blurs the temporal relativity. In contrast, AMP adopts a factorized spatial-temporal attention mechanism and the temporal relativity is encoded with state-of-the art relative encoding technique RoPE [40]. As a result, AMP outperforms MotionLM and StateTransformer, which demonstrates the effectiveness of these designs.

- **Gap is narrowed between autoregressive and independent generation.** Compared to the state-of-the-art MTR++ [38], AMP narrows

Table 3: Ablation Study about Position Encodings.

Method	mAP \uparrow	minADE \downarrow	minFDE \downarrow	MR \downarrow
AMP	0.3581	0.6645	1.4041	0.1717
w/o Spatial	0.3390	0.6968	1.4929	0.1884
Abs Spatial	0.3431	0.6899	1.4633	0.1852
w/o TPE	0.3520	0.6776	1.4349	0.1762
w/o RoPE	0.3492	0.6823	1.4475	0.1840

Table 4: Ablation Study on Training Strategies. F-BN: freezing the statistics of batch norm layer after epoch 30. N-Focal: using those non-static ones among non-focal agents for training. L-Intention: adopting the local intention feature in Eq. 10.

Method	mAP \uparrow	minADE \downarrow	minFDE \downarrow	MR \downarrow
AMP	0.3581	0.6645	1.4041	0.1717
w/o F-BN	0.3248	0.7028	1.5012	0.1968
w/o N-Focal	0.3495	0.6898	1.4622	0.1755
w/o L-Inten	0.3492	0.6712	1.4119	0.1801

down the gap significantly while MotionLM with ensembles lags behind MTR++_Ens by 3 mAP in WOMD and 1.5 mAP in Waymo Interaction.

- **Ensemble is still helpful.** By comparing methods with and without ensemble (MTR - MTRA, MTR++ - MTR++_Ens), we find that ensemble still gives significant performance boosting in the motion prediction field, which demonstrates that current models' performance is far from saturated.

5 Ablation Studies

In this section, we study the effectiveness of the proposed designs with small model and 20% fixed training set of WOMD and we report results on val set.

Effects of Different Position Encodings. Different from MotionLM and StateTransformer, AMP has tailored position encodings for different relations among tokens. In Table 3, we explore the effectiveness of them. We could observe that all position encodings are important. (1) The spatial relative position encoding has the largest impact since it influences all attention mechanisms. Without it, each token is unaware of the relative distance from all other tokens and thus leads to large performance drop. Adopting absolute spatial coordinate system still results in performance drop. (2) Removing the temporal position encoding (TPE) has the least performance degeneration potentially due to the causal mask in the temporal self-attention module leaks information about the number of history tokens before current token, which compensate the functionality of TPE. (3) RoPE is useful as well since it brings awareness about the temporal gap between tokens, which could be useful to estimate movement.

Effects of Training Strategies. Since AMP is a new autoregressive prediction paradigm, unlike the independent generation setting which is well-studied in the community, we find some useful strategies which could stabilize the training

Table 5: Selection of τ for Fuse Function.

τ	mAP \uparrow	minADE \downarrow	minFDE \downarrow	MR \downarrow
0	0.3540	0.6722	1.4044	0.1780
0.5	0.3581	0.6645	1.4041	0.1717
1.0	0.3533	0.6745	1.4102	1.1756

process and improve the performance. Table 4 gives results of ablation studies. (i) We could observe that freezing batch norm statistics at the middle of training could bring explicit performance gains. In our early exploration, we find that the loss fluctuates a lot and we conjecture that the GPT structure may not work well with BN since the original ones in the NLP field does not have BN. Thus, we let BN within PointNets and MLPs collect some statistics to enjoy its benefits [16] in the early epochs and freeze it later for further convergence. (ii) Adding these non-static (with a movement large than 1 meter) non-focal agents to the training set is beneficial, which is opposite to the observations in the independent generation works [20, 36]. (iii) The local intention feature in Eq. 10 could bring extra supervisions which helps the model to distinguish the multiple potential short-term reactions and thus lead to performance gains.

Effects of Fuse Function. As in Eq. 11, the proposed method generates both the short-term $\hat{\mathbf{O}}_{i,t,\text{short}}^k$ and long-term predictions $\hat{\mathbf{O}}_{i,t',\text{long}}^k$. Thus, during inference, the final trajectories could be obtained by fusing the long-term estimation from previous time-steps and the short-term predictions at current time-step. We adopt weighted averaging as in Equ 13:

$$\hat{\mathbf{O}}_{i,t}^k = t^\tau \hat{\mathbf{O}}_{i,t,\text{short}}^k + \sum_{t'=0}^t \frac{t'^\tau}{t^\tau + \sum_{t'=0}^t t'^\tau} \hat{\mathbf{O}}_{i,t',\text{long}}^k [t - t'] \quad (13)$$

where t and t' are the temporal index of current time-step and its previous time-steps respectively, τ is the hyper-parameters where larger τ indicates more weights for short-term predictions. Table 5 shows that the optimal value for τ is the 0.5, which demonstrates the importance of both sides. In future work, more complex fusing functions such as Kalman filter may bring further gains.

6 Implementation Details

We implement the model with Pytorch [31] and the major model has 6 Context Encoder layers and 6 Future Encoder layers with a hidden dimension 512 for fair comparisons with state-of-the-art works [20, 36, 38] while we use a smaller model with 3 Future Encoder layers with a hidden dimension 256 for all ablation studies to save computational resource. Following [36, 38], we generate 64 modes and use the same NMS code to obtain the final 6 trajectories. The model is trained for 50 epochs with an initial learning rate 1e-4, weight decay 5e-3, and clip gradients 1.0. We decay the learning rate by half at epoch 35, 40, 45, 49, 50. Following common GPT training practice, we use Dropout [39] and Droppath [13] rate 0.1 and disable them at the last 2 epochs for convergence.

Additionally, we find that freezing the batch norm layer in the middle epochs (epoch 30 in our experiments) could be helpful for training stability, possibly due to our small batch size (128 in our experiments) limited by the computational resource. As for focal agents, we find that training with those non-static agents could bring performance gains, which is quite different from the observation in the previous works [20, 36]. Thus, during training, we randomly select up to 16 non-static non-focal agents into the training set. For submission to the Leaderboard, we combine train, val, and train20s while for ablation studies we use 20% train set for fast validation.

7 Visualization

We visualize the multi-mode autoregressive prediction results on the Waymo Interaction Dataset in Fig. 5. We could observe that autoregressive prediction generates intention consistent results. Specifically, in Fig. 5a, regarding the left vehicle’s different target, the right vehicle has different speeds. In Fig. 5b, the vehicle’s speed depends on the pedestrian’s speed while in Fig. 5c the vehicle’s speed depends on the pedestrian’s goal point. In Fig. 5d, the two vehicles involved in the cut-in scenario have strong interactions and their future are highly dependent on others.

8 Conclusion

In this work, we propose AMP, an autoregressive motion prediction paradigm based on GPT style next token prediction training, where observed and future states of agents are unanimously represented as tokens in the ego-centric coordinate system. To deal with the complex spatial-temporal and semantic relations among tokens, factorized attention mechanisms with tailored position encodings are proposed. By combining these designs, AMP achieves SOTA performance **Limitations:** Currently, autoregressive prediction’s performance still has small gap with independent generation. Further decoding techniques incorporating classical state estimation methods like Kalman filter could be explored.

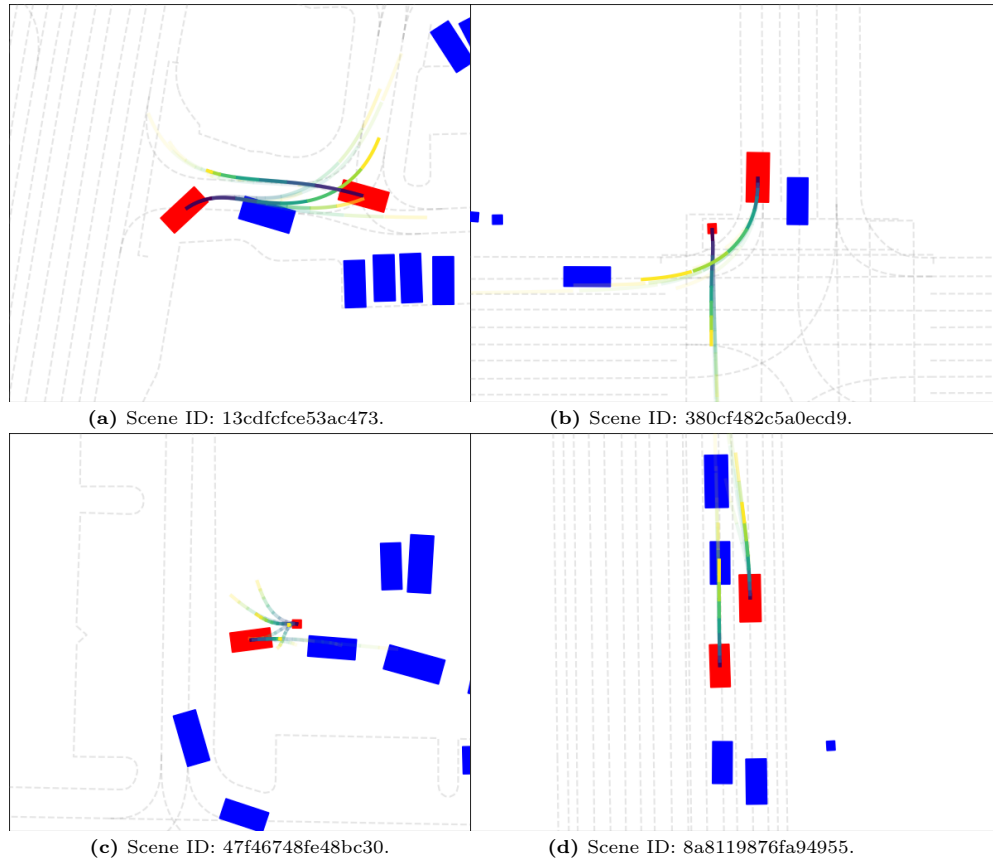


Fig. 5: Visualization of Prediction Results on Validation Set of Waymo Interaction Dataset. We use tokens in different timesteps are in different colors. Modes with higher confidence score would be brighter.

References

1. Alahi, A., Goel, K., Ramanathan, V., Robicquet, A., Fei-Fei, L., Savarese, S.: Social lstm: Human trajectory prediction in crowded spaces. In: CVPR. pp. 961–971 (2016) [2](#), [3](#)
2. Brown, T., Mann, B., Ryder, N., Subbiah, M., Kaplan, J.D., Dhariwal, P., Neelakantan, A., Shyam, P., Sastry, G., Askell, A., Agarwal, S., Herbert-Voss, A., Krueger, G., Henighan, T., Child, R., Ramesh, A., Ziegler, D., Wu, J., Winter, C., Hesse, C., Chen, M., Sigler, E., Litwin, M., Gray, S., Chess, B., Clark, J., Berner, C., McCandlish, S., Radford, A., Sutskever, I., Amodei, D.: Language models are few-shot learners. In: Larochelle, H., Ranzato, M., Hadsell, R., Balcan, M., Lin, H. (eds.) NeurIPS. vol. 33, pp. 1877–1901. Curran Associates, Inc. (2020) [2](#), [3](#), [8](#)
3. Chen, M., Radford, A., Child, R., Wu, J., Jun, H., Luan, D., Sutskever, I.: Generative pretraining from pixels. In: III, H.D., Singh, A. (eds.) Proceedings of the 37th International Conference on Machine Learning. Proceedings of Machine Learning Research, vol. 119, pp. 1691–1703. PMLR (13–18 Jul 2020), <https://proceedings.mlr.press/v119/chen20s.html> [3](#)
4. Cho, K., van Merriënboer, B., Gulcehre, C., Bougares, F., Schwenk, H., Bengio, Y.: Learning phrase representations using rnn encoder-decoder for statistical machine translation. In: Conference on Empirical Methods in Natural Language Processing (EMNLP 2014) (2014) [2](#)
5. Da, F., Zhang, Y.: Path-aware graph attention for hd maps in motion prediction. 2022 International Conference on Robotics and Automation (ICRA) pp. 6430–6436 (2022), <https://api.semanticscholar.org/CorpusID:247158278> [2](#), [4](#)
6. Ettinger, S., Cheng, S., Caine, B., Liu, C., Zhao, H., Pradhan, S., Chai, Y., Sapp, B., Qi, C.R., Zhou, Y., et al.: Large scale interactive motion forecasting for autonomous driving: The waymo open motion dataset. In: ICCV. pp. 9710–9719 (2021) [2](#), [5](#), [8](#), [11](#)
7. Ferruz, N., Schmidt, S., Höcker, B.: Protgpt2 is a deep unsupervised language model for protein design. Nature communications **13**(1), 4348 (2022) [3](#)
8. Gao, J., Sun, C., Zhao, H., Shen, Y., Anguelov, D., Li, C., Schmid, C.: Vectornet: Encoding hd maps and agent dynamics from vectorized representation. In: Proceedings of the IEEE/CVF Conference on Computer Vision and Pattern Recognition. pp. 11525–11533 (2020) [5](#)
9. Gilles, T., Sabatini, S., Tsishkou, D., Stanciulescu, B., Moutarde, F.: Thomas: Trajectory heatmap output with learned multi-agent sampling. In: International Conference on Learning Representations. pp. 1–15 (2022) [4](#)
10. Gu, J., Sun, C., Zhao, H.: Densent: End-to-end trajectory prediction from dense goal sets. In: Proceedings of the IEEE/CVF International Conference on Computer Vision. pp. 15303–15312 (2021) [2](#), [4](#), [12](#)
11. Gupta, A., Johnson, J., Fei-Fei, L., Savarese, S., Alahi, A.: Social gan: Socially acceptable trajectories with generative adversarial networks. In: Proceedings of the IEEE conference on computer vision and pattern recognition. pp. 2255–2264 (2018) [3](#)
12. Hochreiter, S., Schmidhuber, J.: Long short-term memory. Neural computation **9**(8), 1735–1780 (1997) [3](#)
13. Huang, G., Sun, Y., Liu, Z., Sedra, D., Weinberger, K.Q.: Deep networks with stochastic depth. In: Computer Vision–ECCV 2016: 14th European Conference, Amsterdam, The Netherlands, October 11–14, 2016, Proceedings, Part IV 14. pp. 646–661. Springer (2016) [14](#)

14. Huang, Z., Liu, H., Lv, C.: Gameformer: Game-theoretic modeling and learning of transformer-based interactive prediction and planning for autonomous driving. In: Proceedings of the IEEE/CVF International Conference on Computer Vision (ICCV). pp. 3903–3913 (October 2023) [12](#)
15. Huang, Z., Mo, X., Lv, C.: Recoat: A deep learning framework with attention mechanism for multi-modal motion prediction. Workshop on Autonomous Driving, Computer Vision and Pattern Recognition (2021) [4](#)
16. Ioffe, S., Szegedy, C.: Batch normalization: Accelerating deep network training by reducing internal covariate shift. In: International conference on machine learning. pp. 448–456. pmlr (2015) [14](#)
17. Jia, X., Chen, L., Wu, P., Zeng, J., Yan, J., Li, H., Qiao, Y.: Towards capturing the temporal dynamics for trajectory prediction: a coarse-to-fine approach. In: CoRL. pp. 910–920. PMLR (2023) [2, 3](#)
18. Jia, X., Sun, L., Tomizuka, M., Zhan, W.: Ide-net: Interactive driving event and pattern extraction from human data. IEEE Robotics and Automation Letters **6**(2), 3065–3072 (2021). <https://doi.org/10.1109/LRA.2021.3062309> [4](#)
19. Jia, X., Sun, L., Zhao, H., Tomizuka, M., Zhan, W.: Multi-agent trajectory prediction by combining egocentric and allocentric views. In: Faust, A., Hsu, D., Neumann, G. (eds.) Proceedings of the 5th Conference on Robot Learning. Proceedings of Machine Learning Research, vol. 164, pp. 1434–1443. PMLR (08–11 Nov 2022) [4](#)
20. Jia, X., Wu, P., Chen, L., Liu, Y., Li, H., Yan, J.: Hdgt: Heterogeneous driving graph transformer for multi-agent trajectory prediction via scene encoding. IEEE Transactions on Pattern Analysis and Machine Intelligence (TPAMI) (2023) [2, 3, 4, 6, 12, 14, 15](#)
21. Lee, N., Choi, W., Vernaza, P., Choy, C.B., Torr, P.H., Chandraker, M.: Desire: Distant future prediction in dynamic scenes with interacting agents. In: Proceedings of the IEEE/CVF Conference on Computer Vision and Pattern Recognition. pp. 336–345 (2017) [3](#)
22. Liang, M., Yang, B., Hu, R., Chen, Y., Liao, R., Feng, S., Urtasun, R.: Learning lane graph representations for motion forecasting. In: European Conference on Computer Vision. pp. 541–556. Springer (2020) [4](#)
23. Luo, W., Park, C., Cornman, A., Sapp, B., Anguelov, D.: Jfp: Joint future prediction with interactive multi-agent modeling for autonomous driving. In: Conference on Robot Learning. pp. 1457–1467. PMLR (2023) [12](#)
24. Marchetti, F., Becattini, F., Seidenari, L., Bimbo, A.D.: Mantra: Memory augmented networks for multiple trajectory prediction. In: Proceedings of the IEEE/CVF conference on computer vision and pattern recognition. pp. 7143–7152 (2020) [4](#)
25. Mercat, J., Gilles, T., El Zoghby, N., Sandou, G., Beauvois, D., Gil, G.P.: Multi-head attention for multi-modal joint vehicle motion forecasting. In: 2020 IEEE International Conference on Robotics and Automation (ICRA). pp. 9638–9644. IEEE (2020) [2, 4](#)
26. Mildenhall, B., Srinivasan, P., Tancik, M., Barron, J., Ramamoorthi, R., Ng, R.: Nerf: Representing scenes as neural radiance fields for view synthesis. In: European conference on computer vision (2020) [6](#)
27. Mo, X., Huang, Z., Xing, Y., Lv, C.: Multi-agent trajectory prediction with heterogeneous edge-enhanced graph attention network. vol. 23, pp. 9554–9567 (2022). <https://doi.org/10.1109/TITS.2022.3146300> [4](#)

28. Nayakanti, N., Al-Rfou, R., Zhou, A., Goel, K., Refaat, K.S., Sapp, B.: Wayformer: Motion forecasting via simple & efficient attention networks. In: ICRA. pp. 2980–2987. IEEE (2023) [2](#), [12](#)
29. Ngiam, J., Vasudevan, V., Caine, B., Zhang, Z., Chiang, H.T.L., Ling, J., Roelofs, R., Bewley, A., Liu, C., Venugopal, A., et al.: Scene transformer: A unified architecture for predicting future trajectories of multiple agents. In: International Conference on Learning Representations (2021) [4](#), [12](#)
30. OpenAI: Gpt-4 technical report (2023) [3](#)
31. Paszke, A., Gross, S., Massa, F., Lerer, A., Bradbury, J., Chanan, G., Killeen, T., Lin, Z., Gimelshein, N., Antiga, L., Desmaison, A., Kopf, A., Yang, E., DeVito, Z., Raison, M., Tejani, A., Chilamkurthy, S., Steiner, B., Fang, L., Bai, J., Chintala, S.: Pytorch: An imperative style, high-performance deep learning library. In: Advances in Neural Information Processing Systems. vol. 32 (2019) [14](#)
32. Pope, R., Douglas, S., Chowdhery, A., Devlin, J., Bradbury, J., Heek, J., Xiao, K., Agrawal, S., Dean, J.: Efficiently scaling transformer inference. Proceedings of Machine Learning and Systems **5** (2023) [11](#)
33. Qi, C.R., Su, H., Mo, K., Guibas, L.J.: Pointnet: Deep learning on point sets for 3d classification and segmentation. In: Proceedings of the IEEE conference on computer vision and pattern recognition. pp. 652–660 (2017) [5](#)
34. Radford, A., Wu, J., Child, R., Luan, D., Amodei, D., Sutskever, I.: Language models are unsupervised multitask learners (2019) [2](#), [8](#)
35. Seff, A., Cera, B., Chen, D., Ng, M., Zhou, A., Nayakanti, N., Refaat, K.S., Al-Rfou, R., Sapp, B.: Motionlm: Multi-agent motion forecasting as language modeling. In: Proceedings of the IEEE/CVF International Conference on Computer Vision. pp. 8579–8590 (2023) [11](#), [12](#)
36. Shi, S., Jiang, L., Dai, D., Schiele, B.: Motion transformer with global intention localization and local movement refinement. NeurIPS (2022) [2](#), [4](#), [6](#), [9](#), [10](#), [12](#), [14](#), [15](#)
37. Shi, S., Jiang, L., Dai, D., Schiele, B.: Mtr-a: 1st place solution for 2022 waymo open dataset challenge–motion prediction. arXiv preprint arXiv:2209.10033 (2022) [12](#)
38. Shi, S., Jiang, L., Dai, D., Schiele, B.: Mtr++: Multi-agent motion prediction with symmetric scene modeling and guided intention querying. arXiv preprint arXiv:2306.17770 (2023) [2](#), [3](#), [4](#), [6](#), [11](#), [12](#), [14](#)
39. Srivastava, N., Hinton, G., Krizhevsky, A., Sutskever, I., Salakhutdinov, R.: Dropout: A simple way to prevent neural networks from overfitting. Journal of Machine Learning Research **15**(56), 1929–1958 (2014), <http://jmlr.org/papers/v15/srivastava14a.html> [14](#)
40. Su, J., Lu, Y., Pan, S., Murtadha, A., Wen, B., Liu, Y.: Roformer: Enhanced transformer with rotary position embedding. arXiv preprint arXiv:2104.09864 (2021) [3](#), [8](#), [12](#)
41. Sun, Q., Huang, X., Gu, J., Williams, B.C., Zhao, H.: M2i: From factored marginal trajectory prediction to interactive prediction. In: Proceedings of the IEEE/CVF Conference on Computer Vision and Pattern Recognition. pp. 6543–6552 (2022) [12](#)
42. Sun, Q., Zhang, S., Ma, D., Shi, J., Li, D., Luo, S., Wang, Y., Xu, N., Cao, G., Zhao, H.: Large trajectory models are scalable motion predictors and planners (2023) [12](#)
43. Sutskever, I., Vinyals, O., Le, Q.V.: Sequence to sequence learning with neural networks. In: NIPS. Montreal, CA (2014), <http://arxiv.org/abs/1409.3215> [2](#)

44. Tang, C., Salakhutdinov, R.R.: Multiple futures prediction. *Advances in neural information processing systems* **32** (2019) [2](#), [3](#)
45. Touvron, H., Lavril, T., Izacard, G., Martinet, X., Lachaux, M.A., Lacroix, T., Rozière, B., Goyal, N., Hambro, E., Azhar, F., et al.: Llama: Open and efficient foundation language models. *arXiv preprint arXiv:2302.13971* (2023) [8](#)
46. Touvron, H., Martin, L., Stone, K., Albert, P., Almahairi, A., Babaei, Y., Bashlykov, N., Batra, S., Bhargava, P., Bhosale, S., et al.: Llama 2: Open foundation and fine-tuned chat models. *arXiv preprint arXiv:2307.09288* (2023) [8](#)
47. Varadarajan, B., Hefny, A., Srivastava, A., Refaat, K.S., Nayakanti, N., Cornman, A., Chen, K., Douillard, B., Lam, C.P., Anguelov, D., Sapp, B.: Multipath++: Efficient information fusion and trajectory aggregation for behavior prediction. In: *2022 International Conference on Robotics and Automation (ICRA)*. pp. 7814–7821 (2022). <https://doi.org/10.1109/ICRA46639.2022.9812107> [12](#)
48. Vaswani, A., Shazeer, N., Parmar, N., Uszkoreit, J., Jones, L., Gomez, A.N., Kaiser, Ł., Polosukhin, I.: Attention is all you need. *Advances in neural information processing systems* **30** (2017) [3](#), [6](#)
49. Wang, M., Zhu, X., Yu, C., Li, W., Ma, Y., Jin, R., Ren, X., Ren, D., Wang, M., Yang, W.: Ganet: Goal area network for motion forecasting. In: *2023 IEEE International Conference on Robotics and Automation (ICRA)*. pp. 1609–1615 (2023). <https://doi.org/10.1109/ICRA48891.2023.10160468> [2](#), [4](#)
50. Wilson, B., Qi, W., Agarwal, T., Lambert, J., Singh, J., Khandelwal, S., Pan, B., Kumar, R., Hartnett, A., Pontes, J.K., et al.: Argoverse 2: Next generation datasets for self-driving perception and forecasting. In: *NeurIPS Datasets and Benchmarks Track* (2021) [2](#), [5](#), [8](#)
51. Ye, M., Cao, T., Chen, Q.: Tpcn: Temporal point cloud networks for motion forecasting. In: *Proceedings of the IEEE/CVF Conference on Computer Vision and Pattern Recognition*. pp. 11318–11327 (2021) [4](#)
52. Zhang, Z., Liniger, A., Sakaridis, C., Yu, F., Van Gool, L.: Real-time motion prediction via heterogeneous polyline transformer with relative pose encoding. In: *Advances in Neural Information Processing Systems (NeurIPS)* (2023) [12](#)
53. Zhou, Z., Wang, J., Li, Y.H., Huang, Y.K.: Query-centric trajectory prediction. In: *CVPR* (2023) [2](#), [3](#), [4](#), [6](#)
54. Zhou, Z., Wen, Z., Wang, J., Li, Y.H., Huang, Y.K.: Qcnext: A next-generation framework for joint multi-agent trajectory prediction (2023) [2](#), [4](#)
55. Zhou, Z., Ye, L., Wang, J., Wu, K., Lu, K.: Hivt: Hierarchical vector transformer for multi-agent motion prediction. In: *Proceedings of the IEEE/CVF Conference on Computer Vision and Pattern Recognition*. pp. 8823–8833 (2022) [4](#)
56. Zitkovich, B., Yu, T., Xu, S., Xu, P., Xiao, T., Xia, F., Wu, J., Wohlhart, P., Welker, S., Wahid, A., et al.: Rt-2: Vision-language-action models transfer web knowledge to robotic control. In: *7th Annual Conference on Robot Learning* (2023) [3](#)

001 **Supplementary Material for *AMP: Autoregressive*** 001
002 ***Motion Prediction Revisited with Next Token*** 002
003 ***Prediction for Autonomous Driving*** 003

004 Anonymous ECCV 2024 Submission 004

005 Paper ID #6122 005

006 **A Implementation Details** 006

007 We implement the model with Pytorch [?] and the major model has 6 Context 007
008 Encoder layers and 6 Future Encoder layers with a hidden dimension 512 for fair 008
009 comparisons with state-of-the-art works [?, ?, ?] while we use a smaller model 009
010 with 3 Future Encoder layers with a hidden dimension 256 for all ablation studies 010
011 to save computational resource. Following [?, ?], we generate 64 modes and use 011
012 the same NMS code to obtain the final 6 trajectories. The model is trained for 012
013 50 epochs with an initial learning rate 1e-4, weight decay 5e-3, and clip gradients 013
014 1.0. We decay the learning rate by half at epoch 35, 40, 45, 49, 50. Following 014
015 common GPT training practice, we use Dropout [?] and Droppath [?] rate 0.1 015
016 and disable them at the last 2 epochs for convergence. Additionally, we find that 016
017 freezing the batch norm layer in the middle epochs (epoch 30 in our experiments) 017
018 could be helpful for training stability, possibly due to our small batch size (128 in 018
019 our experiments) limited by the computational resource. As for focal agents, we 019
020 find that training with those non-static agents could bring performance gains, 020
021 which is quite different from the observation in the previous works [?, ?]. Thus, 021
022 during training, we randomly select up to 16 non-static non-focal agents into 022
023 the training set. For submission to the Leaderboard, we combine train, val, and 023
024 train20s while for ablation studies we use 20% train set for fast validation. 024

025 **B Visualization** 025

026 We visualize the multi-mode autoregressive prediction results on the Waymo 026
027 Interaction Dataset in Fig. 1. We could observe that autoregressive prediction 027
028 generates intention consistent results. Specifically, in Fig. 1a, regarding the left 028
029 vehicle's different target, the right vehicle has different speeds. In Fig. 1b, the 029
030 vehicle's speed depends on the pedestrian's speed while in Fig. 1c the vehicle's 030
031 speed depends on the pedestrian's goal point. In Fig. 1d, the two vehicles in- 031
032 volved in the cut-in scenario have strong interactions and their future are highly 032
033 dependent on others. 033

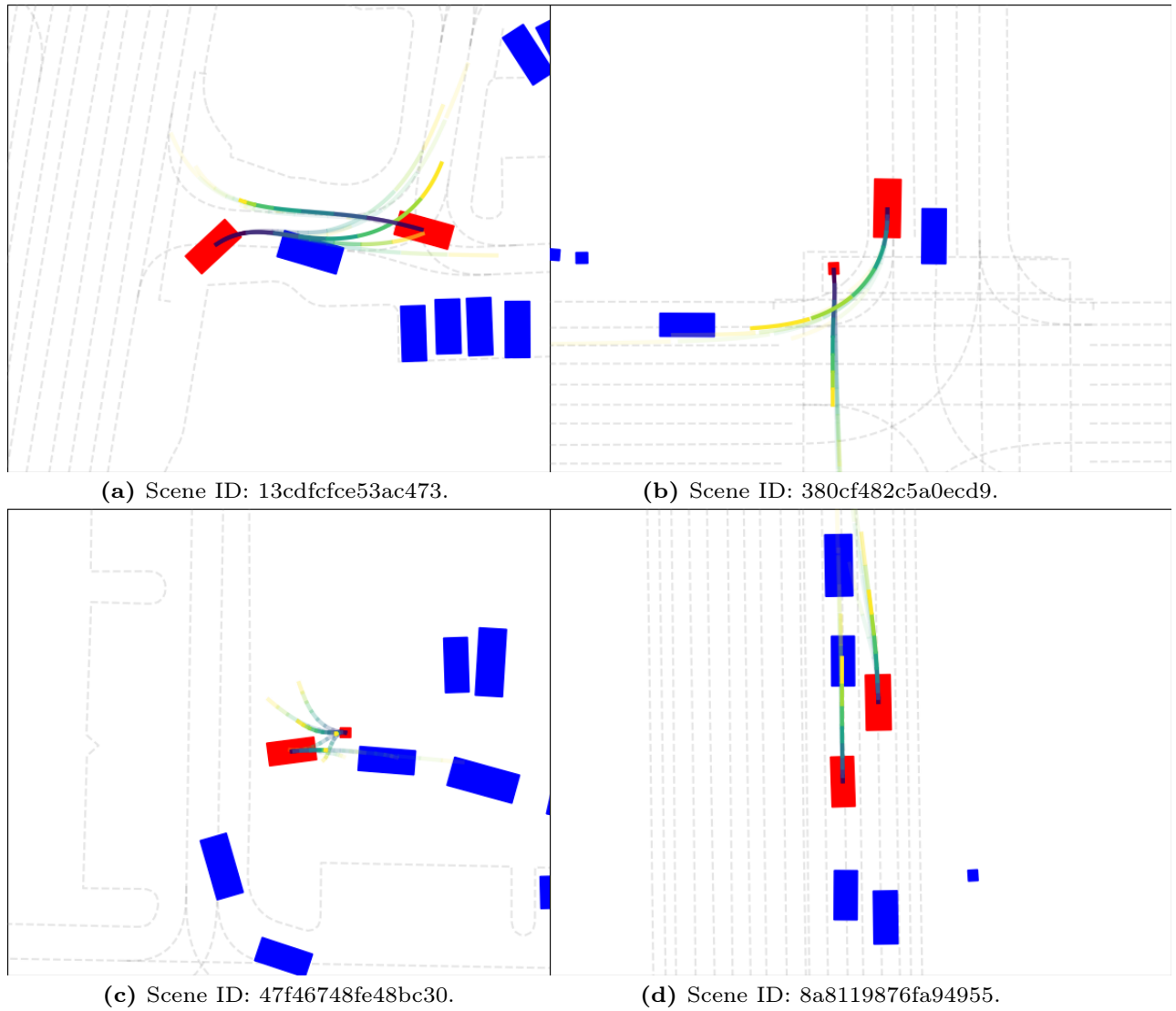


Fig. 1: Visualization of Prediction Results on Validation Set of Waymo Interaction Dataset. We use tokens in different timesteps are in different colors. Modes with higher confidence score would be brighter.